Journal of Materials Chemistry A

COMMUNICATION

View Article Online
View Journal | View Issue

Cite this: J. Mater. Chem. A, 2017, 5, 17211

Received 2nd June 2017
Accepted 25th July 2017

DOI: 10.1039/c7ta04804a

rsc.li/materials-a

A $MnCo_2S_4$ nanowire array as an earth-abundant electrocatalyst for an efficient oxygen evolution reaction under alkaline conditions†

Xiaoping Zhang,[a] Chongdian Si,[b] Xiaoxi Guo,[a] Rongmei Kong[a] and Fengli Qu *[a]

In this communication, we demonstrate the development of a $MnCo_2S_4$ nanowire array directly grown on Ti mesh ($MnCo_2S_4$ NA/TM) as an electrocatalyst for the oxygen evolution reaction in 1.0 M KOH which only needs an overpotential of 325 mV to drive 50 mA cm^{-2}. At an overpotential of 500 mV, this electrocatalyst achieves a high turnover frequency of 0.81 mol O_2 per s.

The energy crisis and environmental issues caused by the excessive consumption of fossil fuels have boosted increasing research interest in the development of clean and renewable energy sources.[1–3] Hydrogen is one such ideal candidate owing to its high energy output and carbon-free combustion products.[4–6] Electrochemical water splitting offers us a promising method for large-scale production of high purity hydrogen.[7–11] However, the sluggish kinetics of the anodic oxygen evolution reaction (OER) generates high overpotential, which is identified as the bottleneck of water splitting for practical applications.[12–15] Thus, highly efficient OER electrocatalysts are required to lower the overpotential.[16–21] RuO_2 and IrO_2 as benchmarking OER catalysts suffer from scarcity and high cost, limiting their widespread commercial applications.[22] Therefore, it is highly attractive to design and develop efficient and low-cost OER catalysts made of earth-abundant elements.[8,23]

Transition metal oxides have been widely recognized as efficient OER electrocatalysts.[24–26] Compared with monometallic ones, bimetallic oxides are more competitive for catalyzing the OER.[27,28] Among bimetallic oxide catalysts, spinel-structured $MnCo_2O_4$ with big cells and a higher number of exposed edge sites, has attracted increasing attention in catalytic and energy storage fields.[29,30] However, its widespread application is still restricted by its limited electrical conductivity. It is reported that sulphospinel materials have higher conductivity and electrochemical activity than the corresponding bimetallic oxides, offering great benefits to enhance electrochemical performances. Recently, Liu *et al.* reported that a $NiCo_2S_4$ nanowire array directly grown on carbon cloth acts as an efficient electrocatalyst for the OER, needing an overpotential of 310 mV to drive 50 mA cm^{-2}.[31] Therefore, $MnCo_2S_4$ is expected to exhibit superior activity to $MnCo_2O_4$. The nanoarray structure favors the improvement of catalytic activity *via* offering a higher number of exposed active sites and facilitating the diffusion of the electrolyte and evolved gas.[32] It is thus highly desirable to develop a $MnCo_2S_4$ nanoarray for the OER, which has never been reported before.

In this communication, we report on the direct growth of a spinel-structured $MnCo_2S_4$ nanowire array on Ti mesh ($MnCo_2S_4$ NA/TM) *via* sulfidation of a $MnCo_2O_4$ nanowire array precursor ($MnCo_2O_4$ NA/TM, see the ESI† for the preparation details). When used as a 3D electrocatalyst for the OER, $MnCo_2S_4$ NA/TM exhibits superior activity and demands an overpotential of only 325 mV to drive a geometric catalytic current density of 50 mA cm^{-2}, which is only 54 mV larger than that of a RuO_2 catalyst. Such $MnCo_2S_4$ NA/TM is also durable with a high turnover frequency of 0.81 mol O_2 per s at an overpotential of 500 mV.

Fig. 1a shows the X-ray diffraction (XRD) patterns of $MnCo_2O_4$ NA/TM and $MnCo_2S_4$ NA/TM. The peaks at 30.5°, 35.9°, 43.8°, 54.3°, 57.9° and 63.6° for $MnCo_2O_4$ NA/TM can be indexed to the (220), (311), (400), (422), (511) and (440) planes of $MnCo_2O_4$ (JCPDS no. 23-1237),[33] respectively. After the sulfidation reaction, the obtained $MnCo_2S_4$ NA/TM shows diffraction peaks at 32.3°, 36.2°, 39.8°, 46.3°, 54.9°, 57.6°, 60.2° and 62.7° indexed to the (200), (210), (211), (220), (311), (222), (230) and (321) crystal planes of $MnCo_2S_4$, respectively, and the other peaks correspond to metallic Ti, which rules out the possibility of other phases. These results demonstrate the successful synthesis of the $MnCo_2S_4$ nanaoarray.[34] The scanning electron microscopy (SEM) image of $MnCo_2O_4$ NA/TM (Fig. 1b) indicates that the entire surface of TM is uniformly coated with

[a]College of Chemistry and Chemical Engineering, Qufu Normal University, Qufu 273165, Shandong, China. E-mail: fengliquhn@hotmail.com

[b]Shandong Engineering Research Center of Chemical Intermediate, Jining University, Qufu 273155, China

† Electronic supplementary information (ESI) available: Experimental section and supplementary figures. See DOI: 10.1039/c7ta04804a

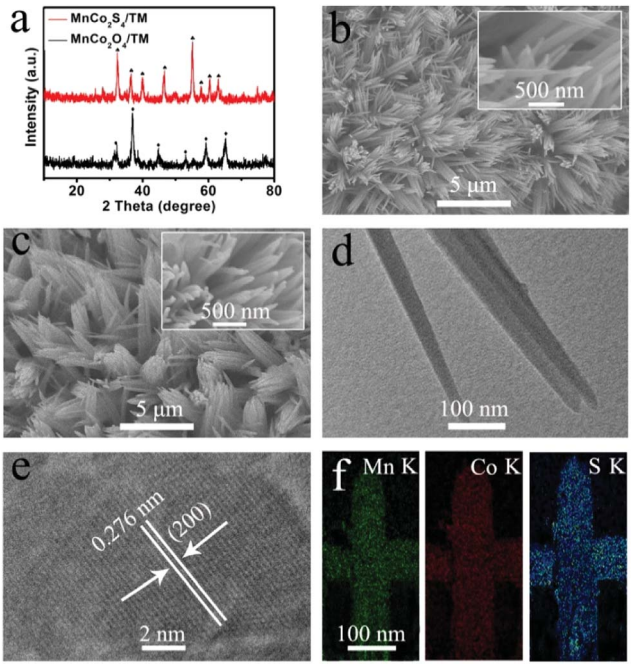

Fig. 1 (a) XRD patterns of $MnCo_2S_4$ NA/TM and $MnCo_2O_4$ NA/TM. SEM images of (b) $MnCo_2O_4$ NA/TM and (c) $MnCo_2S_4$ NA/TM. (d) TEM and (e) HRTEM images of $MnCo_2S_4$. (f) EDX elemental mapping images of Mn, Co, and S elements in $MnCo_2S_4$ NA/TM.

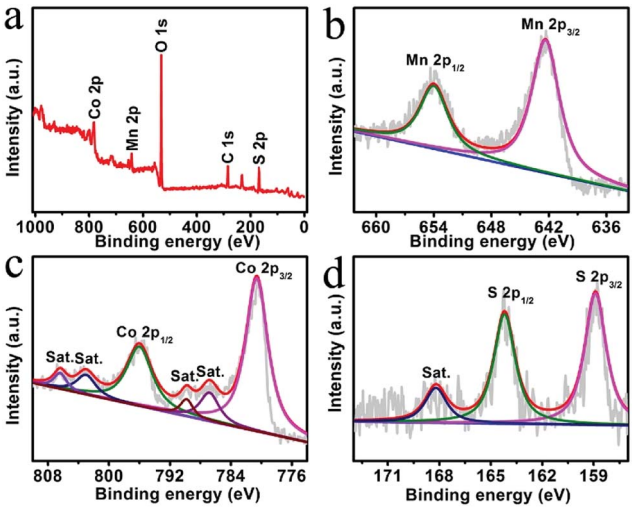

Fig. 2 (a) XPS survey spectrum of $MnCo_2S_4$. XPS spectra of $MnCo_2S_4$ in the (b) Mn 2p, (c) Co 2p, and (d) S 2p regions.

nanowires. It is worth mentioning that the $MnCo_2S_4$ nanowire still maintains the 1D morphology after the sulfidation reaction (Fig. 1c).

As shown in Fig. S2,† the cross-sectional SEM image of $MnCo_2S_4$ NA/TM further reveals that the thickness for this nanoarray is about 7.5 μm. The energy-dispersive X-ray (EDX) spectrum (Fig. S1†) of $MnCo_2S_4$ confirms the existence of Mn, Co, and S elements in the product. Transmission electron microscopy (TEM) analysis of $MnCo_2S_4$ (Fig. 1d and S3†) further suggests that it is a nanowire and not a core–shell structure in nature. Fig. 1e shows the corresponding high-resolution TEM (HRTEM) image, in which the well-resolved lattice fringes with an interplanar distance of 0.276 nm derive from the (200) planes of $MnCo_2S_4$, consistent with the XRD result. The EDX elemental mapping images (Fig. 1f) of $MnCo_2S_4$ NA/TM further suggest the uniform distribution of Mn, Co, and S elements.

Fig. 2a shows the X-ray photoelectron spectroscopy (XPS) survey spectrum of $MnCo_2S_4$, further confirming the presence of Mn, Co, and S elements. The binding energies (BEs) at 654.0 and 642.4 eV in the Mn 2p region (Fig. 2b) are assigned to Mn $2p_{1/2}$ and Mn $2p_{3/2}$, respectively, suggesting the coexistence of Mn^{2+} and Mn^{3+}.[33] In Fig. 2c, the BEs at 780.4 and 796.0 eV in the Co 2p region are ascribed to Co $2p_{3/2}$ and Co $2p_{1/2}$, respectively, and the others peaks are shakeup satellites (identified as "Sat."), suggesting the coexistence of Co^{2+} and Co^{3+}.[35] The S 2p spectrum exhibits two peaks at 164.5 and 158.9 eV. The former represents typical metal–sulphur bonds and the latter is attributed to the sulphur ion in low coordination on the surface (Fig. 2d).[36] According to the XPS analysis, the $MnCo_2S_4$ has a composition of Mn^{2+}, Mn^{3+}, Co^{2+}, Co^{3+} and S^{2-}, which is in good agreement with results reported in previous studies.[37] No change is observed for the XPS spectra of $MnCo_2S_4$ NA/TM in Mn 2p and S 2p regions after OER electrolysis (Fig. S4†). Two peaks at 781.6 and 797.4 eV corresponding to Co $2p_{3/2}$ and Co $2p_{1/2}$ in $Co(OH)_2$, respectively. It indicates that the characteristic peaks exhibit positive shifts of 1.2 and 1.4 eV, respectively. Thus, we conclude that $Co(OH)_2$ is formed at the surface of $MnCo_2S_4$ NA/TM.[31]

The OER activity of $MnCo_2S_4$ NA/TM ($MnCo_2S_4$ loading: 1.78 mg cm^{-2}) was measured in 1.0 M KOH using a typical three-electrode system with a scan rate of 5 mV s^{-1}. For comparison, bare TM, $MnCo_2O_4$ NA/TM and RuO_2/TM were also tested under the same conditions. Due to the presence of ohmic potential drop (*iR*), the as-measured reaction currents cannot directly reflect the intrinsic behavior of catalysts. Thus, an *iR* correction was applied to all initial data for further analysis and all the data were reported on a reversible hydrogen electrode (RHE) scale unless particularly stated. Fig. 3a presents the linear sweep voltammetry (LSV) curves. As expected, RuO_2/TM is highly active for water oxidation with the need for an overpotential of 271 mV to achieve 50 mA cm^{-2}, whereas bare TM has almost no OER activity. Note that $MnCo_2S_4$ NA/TM shows excellent OER performance with an overpotential of 325 mV to drive a catalytic current density of 50 mA cm^{-2}, 368 mV less than that of $MnCo_2O_4$ NA/TM (693 mV). $MnCo_2S_4$ NA/TM needs an overpotential of 613 mV to drive 50 mA cm^{-2} in 0.1 M KOH. Our $MnCo_2S_4$ NA/TM also compares favorably with the behaviors of reported non-noble-metal OER catalysts in alkaline media (Table S1†). In commercial alkaline water electrolysers, OER catalysts need to meet strict conditions usually operated in 25–30 wt% KOH.[19] We thus test the OER activity of $MnCo_2S_4$ NA/TM in 30 wt% KOH. Fig. S8† shows that $MnCo_2S_4$ NA/TM exhibits higher current density and lower onset overpotential than those measured in 1.0 M KOH, with the demand of an overpotential of 144 mV to attain 50 mA cm^{-2}. This overpotential is significantly less than the reported value.[10,38]

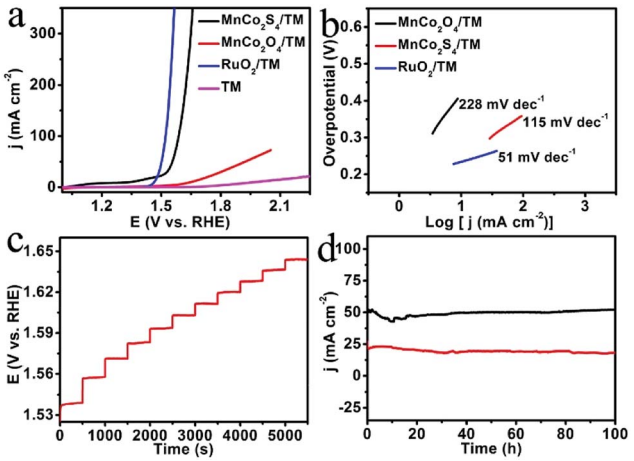

Fig. 3 (a) LSV curves of $MnCo_2S_4$ NA/TM, $MnCo_2O_4$ NA/TM, RuO_2/TM, and bare TM with a scan rate of 5 mV s^{-1}. (b) Tafel plots of $MnCo_2S_4$ NA/TM, $MnCo_2O_4$ NA/TM, and RuO_2/TM. (c) Multi-current process for $MnCo_2S_4$ NA/TM. The current density started at 20 mA cm^{-2}, and ended at 120 mA cm^{-2}, with an increment of 10 mA per cm^2 per 500 s without *iR* correction. (d) Time-dependent current density curves of $MnCo_2S_4$ NA/TM in 1.0 M KOH.

Fig. 3b shows the Tafel plots of catalysts. RuO_2/TM exhibits a Tafel slope of 51 mV dec^{-1} in the region of 1.458–1.494 V. The $MnCo_2O_4$ NA/TM exhibits a Tafel slope of 228 mV dec^{-1} in the region of 1.538–1.637 V. In contrast, $MnCo_2S_4$ NA/TM exhibits a much smaller Tafel slope of 115 mV dec^{-1} in the region of 1.525–1.589 V, implying faster OER kinetics of the $MnCo_2S_4$ NA/TM electrocatalyst. The high Tafel slopes can be due to the difference in the catalytic structure, in the resistance of materials and in charge transfer on and within the catalysts.[39] The OER in alkaline solution consists of the following three steps:

$$M + H_2O \rightleftharpoons M\text{–}OH + H^+ + e^- \quad (1)$$

$$M\text{–}OH \rightleftharpoons M\text{–}O + H^+ + e^- \quad (2)$$

$$M\text{–}O \rightleftharpoons M + O_2. \quad (3)$$

Where M represents the electrocatalysts. A Tafel slope of 120, 40, or 15 mV dec^{-1} would be expected if the step (1), step (2), or step (3) is the rate-determining step, respectively.[40,41] Thus, step (1) is the rate-determining step for the OER on $MnCo_2S_4$ NA/TM. The multi-step chronopotentiometric curve of $MnCo_2S_4$ NA/TM with the current density increased from 20 to 120 mA cm^{-2} (10 mA per cm^2 per 500 s) is displayed in Fig. 3c. Stability is a significant parameter to evaluate the practicability of electrocatalysts. Fig. 3d shows the time-dependent current density curves at fixed current densities of 20 and 50 mA cm^{-2}. As observed, $MnCo_2S_4$ NA/TM maintains its catalytic activity for at least 100 h at both current densities in 1.0 M KOH, suggesting its high electrochemical stability. We also investigated LSV curves of $MnCo_2S_4$ NA/TM before and after 500 cyclic voltammetry cycles. As observed, this electrode shows negligible current loss after 500 cycles in 1.0 M KOH (Fig. S5†), indicating the high stability of $MnCo_2S_4$ NA/TM. We further estimated the electrochemically active surface area (ECSA) of $MnCo_2S_4$ NA/TM and $MnCo_2O_4$ NA/TM by determining the double-layer capacitance (C_{DL}) of the systems *via* cyclic voltammetry (Fig. 4) according to previous reports.[42,43] The capacitances of $MnCo_2S_4$ NA/TM and $MnCo_2O_4$ NA/TM are measured to be 9.5 and 1.55 mF cm^{-2}, respectively, suggesting a much higher surface roughness and surface area of $MnCo_2S_4$ NA/TM.

We also employed turnover frequency (TOF), associated with generating oxygen molecules per second, to further investigate the intrinsic activity of the as-prepared electrocatalysts at a fixed overpotential.[44] To calculate the TOF, the concentration of active sites needs to be quantified through electrochemistry according to reported work.[45] As presented in Fig. S6,† we observe a linear dependence between the plot of the oxidation current for redox species and scan rates from cyclic voltammograms (CVs). The slope is given by the formula: slope $= n^2F^2m/4RT$, where n representing the number of electrons transferred is 1 assuming a one-electron process for oxidation of metal centers in $MnCo_2S_4$ NA/TM and $MnCo_2O_4$ NA/TM, F is the faradaic constant (96 485 C mol^{-1}), m is the number of active species, and R and T are the ideal gas constant and the absolute temperature, respectively. The TOF was then calculated by the following equation: TOF $= JA/4Fm$, where J is the current density, A is the geometrical electrode area, and 4 expresses the moles of electron consumption for one mole O_2 evolution. Thus we obtained the TOF of $MnCo_2S_4$ NA/TM as 0.81 mol O_2 per s at an overpotential of 500 mV, much larger than 0.05 mol O_2 per s for $MnCo_2O_4$ NA/TM at the same overpotential (Fig. S7†).

The faradaic efficiency (FE) of $MnCo_2S_4$ NA/TM was determined by gas chromatography analysis and measured quantitatively using a calibrated pressure sensor to monitor the pressure change in an anode compartment of the H-type electrolytic cell. Fig. S9† shows the amount of O_2 produced at 1.51 V in 1.0 M KOH, indicating that the volume of O_2 increases during continuous electrolysis. The FE of the electrocatalytic oxygen

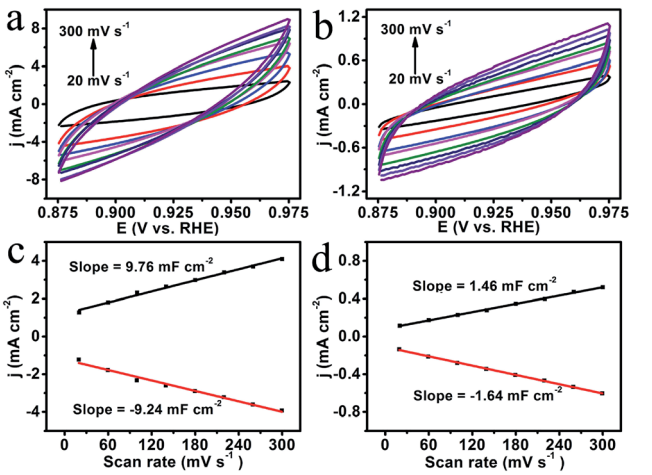

Fig. 4 CVs of (a) $MnCo_2S_4$ NA/TM and (b) $MnCo_2O_4$ NA/TM in the non-faradaic capacitance current range at scan rates of 20, 60, 100, 140, 180, 220, 260 and 300 mV s^{-1}. (c and d) Corresponding capacitive currents of scan rates for $MnCo_2S_4$ NA/TM and $MnCo_2O_4$ NA/TM in 1.0 M KOH, respectively.

evolution process in alkaline solution was calculated to be 97.2%.

In summary, a $MnCo_2S_4$ nanowire array was successfully developed on TM through sulfurization of the corresponding $MnCo_2O_4$ nanowire array precursor. As a durable bimetallic water oxidation electrocatalyst, $MnCo_2S_4$ NA/TM shows high catalytic activity and reproducibility, with the need for an overpotential of 325 mV to drive a geometric current density of 50 mA cm^{-2} in 1.0 M KOH, as efficient as the reported $NiCo_2S_4$ nanowire array supported on carbon cloth (needing 310 mV to afford 50 mA cm^{-2}). It also demonstrates strong long-term electrochemical durability with a high TOF of 0.81 mol O_2 per s at an overpotential of 500 mV. In 30 wt% KOH, a small overpotential of 144 mV is needed to attain 50 mA cm^{-2}. This work is important because it not only provides us an attractive catalyst material for efficient and durable electrochemical water oxidation in alkaline media, but also would open up an exciting new avenue for the rational design and fabrication of Mn-based sulphide nanoarrays for applications. This catalyst is also promising for other sensing applications.[46]

Conflict of interest

There are no conflicts of interest to declare.

Acknowledgements

This work was supported by the National Natural Science Foundation of China (21375076), the Key Research and Development Program of Shandong Province (2015GSF121031), the China Postdoctoral Science Foundation funded project (2017M610406) and the key research and development plan of Jining city.

References

1 J. Chow, R. J. Kopp and P. R. Portney, *Science*, 2003, **302**, 1528–1531.
2 Y. Zheng, Y. Jiao, Y. Zhu, L. Li, Y. Han, Y. Chen, A. Du, M. Jaroniec and S. Qiao, *Nat. Commun.*, 2014, **5**, 3783.
3 J. Yang, D. Wang, H. Han and C. Li, *Acc. Chem. Res.*, 2013, **46**, 1900–1909.
4 R. F. Service, *Science*, 2009, **324**, 1257–1259.
5 J. Tian, Q. Liu, A. M. Asiri and X. Sun, *J. Am. Chem. Soc.*, 2014, **136**, 7587–7590.
6 T. Liu, Q. Liu, A. M. Asiri, Y. Luo and X. Sun, *Chem. Commun.*, 2015, **51**, 16683–16686.
7 J. R. Mckone, S. C. Marinescu, B. S. Brunschwig, J. R. Winkler and H. B. Gray, *Chem. Sci.*, 2014, **5**, 865–878.
8 J. Wang, W. Cui, Q. Liu, Z. Xing, A. M. Asiri and X. Sun, *Adv. Mater.*, 2016, **28**, 215–230.
9 T. Liu, A. M. Asiri and X. Sun, *Nanoscale*, 2016, **8**, 3911–3915.
10 L. Xie, C. Tang, K. Wang, G. Du, A. M. Asiri and X. Sun, *Small*, 2017, **13**, 1602755.
11 S. Hao and Y. Yang, *J. Mater. Chem. A*, 2017, **5**, 12091–12095.
12 Q. Yin, J. M. Tan, C. Besson, Y. V. Geletii, D. G. Musaev, A. E. Kuznetsov, Z. Luo, K. I. Hardcastle and C. L. Hill, *Science*, 2010, **328**, 342–345.
13 L. Xie, R. Zhang, L. Cui, D. Liu, S. Hao, Y. Ma, G. Du, A. M. Asiri and X. Sun, *Angew. Chem., Int. Ed.*, 2017, **56**, 1064–1068.
14 J. Suntivich, K. J. May, H. A. Gasteiger, J. B. Goodenough and S.-H. Yang, *Science*, 2011, **334**, 1383–1385.
15 N. Cheng, Q. Liu, J. Tian, Y. Xue, A. M. Asiri, H. Jiang, Y. He and X. Sun, *Chem. Commun.*, 2015, **51**, 1616–1619.
16 M. Yu, L. Jiang and H. Yang, *Chem. Commun.*, 2015, **51**, 14361–14364.
17 T. Ma, S. Dai, M. Jaroniec and S. Qiao, *Angew. Chem., Int. Ed.*, 2014, **53**, 7281–7285.
18 P. Chen, K. Xu, Z. Fang, Y. Tong, J. Wu, X. Lu, X. Peng, H. Ding, C. Wu and Y. Xie, *Angew. Chem., Int. Ed.*, 2015, **54**, 14710–14714.
19 C. Tang, A. M. Asiri and X. Sun, *Chem. Commun.*, 2016, **5**, 4529–4532.
20 N. Cheng, Q. Liu, A. M. Asiri, W. Xing and X. Sun, *J. Mater. Chem. A*, 2015, **3**, 23207–23212.
21 C. Tang, N. Cheng, Z. Pu, W. Xing and X. Sun, *Angew. Chem., Int. Ed.*, 2015, **54**, 9351–9355.
22 Y. Lee, J. Suntivich, K. J. May, E. E. Perry and Y. Shao-Horn, *J. Phys. Chem. Lett.*, 2012, **3**, 399–404.
23 S. Du, Z. Ren, J. Zhang, J. Wu, W. Xi, J. Zhu and H. Fu, *Chem. Commun.*, 2015, **51**, 8066–8069.
24 L. Han, S. Dong and E. Wang, *Adv. Mater.*, 2016, **28**, 9266–9291.
25 C. H. Kuo, I. M. Mosa, S. Thanneeru, V. Sharma, L. Zhang, S. Biswas, M. Aindow, S. P. Alpay, J. F. Rusling, S. L. Suib and J. He, *Chem. Commun.*, 2015, **51**, 5951–5954.
26 D. Wang, X. Chen, D. G. Evans and W. Yang, *Nanoscale*, 2013, **5**, 5312–5315.
27 R. D. L. Smith, M. S. Prevot, R. D. Fagan, Z. Zhang, P. A. Sedach, M. K. J. Siu, S. Trudel and C. P. Berlinguette, *Science*, 2013, **340**, 60–63.
28 X. Liu, Z. Chang, L. Luo, T. Xu, X. Lei, J. Liu and X. Sun, *Chem. Mater.*, 2014, **26**, 1889–1895.
29 X. Ge, Y. Liu, F. W. T. Goh, T. S. A. Hor, Y. Zong, P. Xiao, Z. Zhang, S. H. Lim, B. Li, X. Wang and Z. Liu, *ACS Appl. Mater. Interfaces*, 2014, **6**, 12684–12691.
30 C. Xiao, X. Zhang, T. Mendes, G. P. Knowles, A. Chaffee and D. R. MacFarlane, *J. Phys. Chem. C*, 2016, **120**, 23976–23983.
31 D. Liu, Q. Lu, Y. Luo, X. Sun and A. M. Asiri, *Nanoscale*, 2015, **7**, 15122–15126.
32 Y. Liang, Q. Liu, Y. Luo, X. Sun, Y. He and A. M. Asiri, *Electrochim. Acta*, 2016, **190**, 360–364.
33 S. Ma, L. Sun, L. Cong, X. Gao, C. Yao, X. Guo, L. Tai, P. Mei, Y. Zeng, H. Xie and R. Wang, *J. Phys. Chem. C*, 2013, **117**, 25890–25897.
34 S. Liu and S. C. Jun, *J. Power Sources*, 2017, **342**, 629–637.
35 S. Wang, Y. Hou and X. Wang, *ACS Appl. Mater. Interfaces*, 2015, **7**, 4327–4335.
36 Y. Liu, J. Zhang, S. Wang, K. Wang, Z. Chen and Q. Xu, *New J. Chem.*, 2014, **38**, 4045–4048.

37 A. M. Elshahawy, X. Li, H. Zhang, Y. Hu, K. Ho, C. Guan and J. Wang, *J. Mater. Chem. A*, 2017, **5**, 7494–7506.
38 N. Yang, C. Tang, K. Wang, G. Du, A. M. Asiri and X. Sun, *Nano Res.*, 2016, **9**, 3346–3354.
39 K. Xu, P. Chen, X. Li, Y. Tong, H. Ding, X. Wu, W. Chu, Z. Peng, C. Wu and Y. Xie, *J. Am. Chem. Soc.*, 2015, **137**, 4119–4125.
40 A. T. Marshall and L. V. Bethune, *Electrochem. Commun.*, 2015, **61**, 23–26.
41 X. Zou, Y. Liu, G. Li, Y. Wu, D. Liu, W. Li, H. Li, D. Wang, Y. Zhang and X. Zou, *Adv. Mater.*, 2017, **29**, 1700404.
42 S. Hao, L. Yang, D. Liu, R. Kong, G. Du, A. M. Asiri, Y. Yang and X. Sun, *Chem. Commun.*, 2017, **53**, 5710–5713.
43 C. C. L. McCrory, S. Jung, J. C. Peters and T. F. Jaramillo, *J. Am. Chem. Soc.*, 2013, **135**, 16977–16987.
44 R. M. Ramsundar, J. Debgupta, V. K. Pillai and P. A. Joy, *Electrocatalysis*, 2015, **6**, 331–340.
45 Y. Li, L. Zhang, X. Xiang, D. Yan and F. Li, *J. Mater. Chem. A*, 2014, **2**, 13250–13258.
46 J. Tian, N. Cheng, Q. Liu, W. Xing and X. Sun, *Angew. Chem., Int. Ed.*, 2015, **54**, 5493–5497.